Global Change Biology

Global Change Biology (2016) **22**, 2125–2137, doi: 10.1111/gcb.13227

Wood anatomy and carbon-isotope discrimination support long-term hydraulic deterioration as a major cause of drought-induced dieback

ELENA PELLIZZARI[1], J. JULIO CAMARERO[2], ANTONIO GAZOL[2], GABRIEL SANGÜESA-BARREDA[2] and MARCO CARRER[1]

[1]*Dip. TeSAF, Universitá degli Studi di Padova, Agripolis I-35020, Legnaro, Italy,* [2]*Instituto Pirenaico de Ecología (IPE-CSIC), Avda Montañana 1005, Zaragoza 50059, Spain*

Abstract

Hydraulic impairment due to xylem embolism and carbon starvation are the two proposed mechanisms explaining drought-induced forest dieback and tree death. Here, we evaluate the relative role played by these two mechanisms in the long-term by quantifying wood-anatomical traits (tracheid size and area of parenchyma rays) and estimating the intrinsic water-use efficiency (iWUE) from carbon isotopic discrimination. We selected silver fir and Scots pine stands in NE Spain with ongoing dieback processes and compared trees showing contrasting vigour (declining vs nondeclining trees). In both species earlywood tracheids in declining trees showed smaller lumen area with thicker cell wall, inducing a lower theoretical hydraulic conductivity. Parenchyma ray area was similar between the two vigour classes. Wet spring and summer conditions promoted the formation of larger lumen areas, particularly in the case of nondeclining trees. Declining silver firs presented a lower iWUE than conspecific nondeclining trees, but the reverse pattern was observed in Scots pine. The described patterns in wood anatomical traits and iWUE are coherent with a long-lasting deterioration of the hydraulic system in declining trees prior to their dieback. Retrospective quantifications of lumen area permit to forecast dieback in declining trees 2–5 decades before growth decline started. Wood anatomical traits provide a robust tool to reconstruct the long-term capacity of trees to withstand drought-induced dieback.

Keywords: Abies alba, dendrochronology, dieoff, hydraulic conductivity, parenchyma, *Pinus sylvestris*, quantitative wood anatomy, water-use efficiency, xylem

Received 10 September 2015; revised version received 23 December 2015 and accepted 30 December 2015

Introduction

Forests store almost half of the terrestrial carbon (Bonan, 2008), and most of this sink corresponds to lasting woody pools that contribute to mitigate the ongoing rise of atmospheric CO_2 (Pan *et al*., 2011). However, there is growing concern about the fate of some forests in drought-prone areas because increasing frequency and intensity of climate extremes, such as heat waves and prolonged droughts, can make some stands particularly vulnerable to water deficit (Bréda *et al*., 2006; Allen *et al*., 2010; Allen *et al*. 2015). Global forest die-off in response to drought illustrates how rapidly some forest ecosystem services may be partially lost, such as the ability to sequester carbon due to fast vigour loss, growth decline, and increasing mortality rates (Anderegg 2015).

The physiology of drought-induced dieback and tree mortality likely involves failures of the coupled hydraulic system and carbon dynamics (McDowell, 2011; Sala *et al*., 2012). Drought stress acts on several tree processes that are usually interrelated. For instance, stomatal closure prevents xylem embolism but reduces carbon uptake, which impairs phloem functioning and decreases the availability of sugar osmolytes (Sevanto *et al*., 2014). Drought stress constrains and also uncouples growth and photosynthesis (Hsiao, 1973), and such decoupling could increase the concentrations of nonstructural carbohydrates in tissues of drought-stressed trees (Körner, 2003; but see Galiano *et al*., 2011). Traits such as wood density and anatomy, often linked to hydraulic conductivity, also determine how vulnerable species and trees are to dieoff by affecting xylem embolism, growth and carbon use (Hoffmann *et al*., 2011; Anderegg, 2015).

Wood formation reflects changes in forest productivity and carbon sequestration (Babst *et al*., 2014), but it also captures changes in tree vigour since water shortage usually induces the formation of narrow tree rings (Dobbertin, 2005). Wood anatomical features such as lumen area (a proxy for the theoretical hydraulic conductivity provided by each tracheid (von Wilpert, 1991;

Correspondence: J. Julio Camarero, tel. +34 976 369393, fax+34 976 716019, e-mail: jjcamarero@ipe.csic.es

Cuny *et al*., 2014)) or cell-wall thickness (closely related to xylem carbon costs) are useful proxies to quantify the long-term tree responses to drought stress (Fonti *et al*., 2010). Nonetheless, quantitative wood anatomy has been little exploited to infer the relative importance played by the physiological mechanisms proposed to explain drought-triggered die-off (but see Levanič *et al*., 2011; Hereş *et al*., 2014) and often with contrasting findings. For instance, some authors reported a drought-reduced lumen area leading to a decline in stem hydraulic conductivity (Bryukhanova & Fonti, 2013; Liang *et al*., 2013), whilst others found the opposite (Eilmann *et al*., 2009, 2011; Martin-Benito *et al*., 2013). This evidences that growth responses to drought are complex due to contingency on tree features such as age, size and species-specific traits. We hypothesize that quantitative wood anatomy, a loosely explored field, may help to advance our knowledge in this topic.

Most mechanistic approaches investigating drought-induced forest dieback focus mainly on the short-term processes such as altered hydraulic functions or loss in carbon uptake (McDowell *et al*., 2008). For instance, tree hydraulic performance in conifers is usually restricted to the last 10–20 rings which encompass the most active sapwood (Sperry & Love, 2015), even if in some species the number of sapwood rings can be up to 50 (Knapic & Pereira, 2005). But trees are long-lived organisms whose susceptibility to extreme droughts can change in parallel with the corresponding long-term variability in climate or stand features (e.g. rising temperature, increase evapotranspiration, increasing competition, etc.). Within this context, time series of wood-anatomical features combined with carbon isotopes can provide a long-term record suitable to assess how trees are predisposed to drought-induced die-off.

Long-term variability in xylem anatomical traits can be related not only to ontogeny (Carrer *et al*., 2015), but also to carbon fixation and water exchange by analyzing the corresponding changes in intrinsic water-use efficiency (iWUE) derived from carbon-isotope discrimination of tree-ring wood (Saurer *et al*., 2004). The iWUE is a proxy of the amount of water loss at the leaf level due to stomatal conductance per unit of assimilated carbon (Seibt *et al*., 2008). Increases in iWUE may respond to greater photosynthetic efficiency due to reduced rates of photorespiration at high leaf-internal CO_2 concentration, reduced water loss due to stomata closure, or both (Lévesque *et al*., 2013). Rising CO_2 reduces stomatal conductance and decreases water loss, and in some cases leads to larger lumen areas or increases latewood density (Yazaki *et al*., 2005). However, fertilization effects on growth due to rising CO_2, postulated to be stronger on forests located in dry areas, have not been documented in drought-prone areas (McDowell, 2011; Linares & Camarero, 2012). Hence, the long-term characterization of iWUE can help to disentangle the photosynthetic and hydraulic responses in trees experiencing drought-induced dieback.

Here, we aim to investigate the trees hydraulic performances at the same time scale of their lifespan. Our target is to gain knowledge on the different responses of tree species to drought-triggered die-off by analysing and comparing the long-term changes in some wood anatomical traits and carbon-isotope discrimination of declining and nondeclining Scots pine and silver fir trees. As successive droughts may lead to accumulated hydraulic conductance loss in declining trees (Anderegg *et al*., 2013), we hypothesize that these trees are characterized by a lower hydraulic conductivity than nondeclining ones. Specifically, we expect that declining trees will produce earlywood tracheids, which account for most of the ring conductivity, with smaller lumen area than nondeclining trees. We also expect that nondeclining trees will show an improved iWUE due to reduced water loss per unit carbon gain as compared to declining trees. Investigating how trees react to drought will help to forecast which forests will be the most vulnerable in coupled carbon-climate-vegetation models (Bréda *et al*., 2006). This will be particularly useful in the Mediterranean Basin and other areas subjected to season water shortage where future climate scenarios predict an increased frequency of extreme droughts (IPCC, 2014).

Materials and methods

Study sites and tree species

In early 2012, we selected two sites in NE Spain (Aragón) dominated by silver fir (*Abies alba*) and Scots pine (*Pinus sylvestris*) and significantly affected by the 2012 drought with abundant defoliated and dying trees (Camarero *et al*., 2015). The selection of two species allowed comparison of their different wood-anatomical and growth responses to the severe drought. The climate at both sites is continental Mediterranean, however, the silver fir site is mesic (mean annual temperature 9.9 °C, total precipitation 1066 mm and annual water balance 531 mm), whereas the Scots pine site is xeric (mean annual temperature 11.8 °C, total precipitation 375 mm and annual water balance −210 mm). Regarding the regulation of water status, the species' stomatal strategy is relatively isohydric, even if isohydry and anisohydry strategies are likely a continuum (Klein, 2014).

Field sampling

The two stands presented many defoliated and dying trees of the two dominant species after the 2012 drought, which was

the most severe (<mean -SD if expressed as drought indices) in NE Spain since 1950 (Trigo *et al*., 2013; Camarero *et al*., 2015). We measured size variables (dbh, diameter at breast height measured at 1.3 m; height) and defoliation status in 38 trees per species to characterize the die-off pattern. To describe tree vigour we estimated the percentage of crown defoliation using binoculars (Dobbertin, 2005). Trees showing <50% postdrought defoliation were considered to be nondeclining, whereas trees with ≥50% postdrought defoliation were considered as declining. This represented a more robust criterion to differentiate declining from nondeclining trees than those based on radial-growth data (Camarero *et al*., 2015). We randomly selected five trees per vigour class in each species. We then estimated the current competition-intensity index (Camarero *et al*., 2011) of each tree by measuring the neighbourhood basal area of all woody species with height ≥1.3 m. The neighbourhood was defined as a circular area located within an 8-m wide circle centred on each focal tree (see Sangüesa-Barreda *et al*., 2015). We obtained monthly and seasonal climatic variables for the 1950–2012 period [mean maximum and minimum temperatures, precipitation (P), estimated potential evapotranspiration (PET) and water balance (P-PET)] from meteorological stations located near the sampling sites (*cf*. Camarero *et al*., 2015 for further details on site characteristics, sampling design and climate data).

Processing of wood samples

Trees were cored at 1.3 m using a 10-mm Pressler increment borer. First, we divided the cores in 3–5 cm long blocks, which were boiled in water to soften them and remove resins. We then used a rotary microtome (Leica RM 2255; Leica Microsystems, Germany) to cut transverse and tangential wood sections (15–20 μm thick) for the respective measurements of the tracheid (dimensions) and parenchyma (area) variables. Wood sections were stained by mixing safranin (1%) and astra blue (0.5%) solutions. They were then fixed and permanently mounted onto glass microscope slides using a synthetic resin (Eukitt™; Merck, Darmstadt, Germany). Digital images were captured at 100× with a digital camera attached to a light microscope. We created panoramas stitching together multiple overlapping images using the PtGui software. Finally, images were processed using the ROXAS software (von Arx & Carrer, 2014), specifically developed for the analysis of long series of wood-anatomical features.

In the analyses of wood-anatomical traits we avoided tissue anomalies such as compression wood or callus tissue. Furthermore, the selected cores contained the innermost rings located close to the pith to ensure the measurement of the whole ontogenetic sequence of wood formation. We considered 10 trees per species for the transverse measures, while six trees (three declining plus three nondeclining trees) were processed in the tangential measures.

Wood anatomy data

All tracheids forming a ring were measured across transverse sections, but the resulting variables were quantified at the whole ring level or separately for the earlywood and latewood. Sections were ca. 10-μm thick. The identification of earlywood, transition wood and latewood was based on the ring division in five sectors according to the position of each cell within the ring, and based on a Principal Component Analysis calculated on the sectors' time series (Figs S1 and S2). This separation was preferred over the delineation based on the Mork index (Denne, 1988) for its higher efficiency in defining earlywood and latewood in conifers within the Mediterranean region (e.g. Pacheco *et al*., 2015). Variables measured included ring width, number of tracheids forming a ring, their mean lumen area and cell-wall thickness (henceforth CWT), computed as the average between the tangential and radial thicknesses. Using these variables, we calculated the annual theoretical hydraulic conductivity (K_h) according to the Hagen-Poiseuille law, which states that the capillary flow rate is proportional to the square of the conduit area (Tyree & Zimmermann, 2002). We also calculated the cell-wall thickness-to-span ratio [$(CWT/LD)^2$] where LD is the mean lumen diameter calculated as the average between radial and tangential internal cell diameter. This ratio is assumed to be a surrogate of the xylem resistance against embolism, since it considers both cell wall thickness (mechanical properties) and lumen diameter (hydraulic properties), and it is usually linked to wood density (Hacke *et al*., 2001). Finally, we estimated the carbon cost investment of tracheid formation (C_{cost}) by multiplying the number of tracheids by CWT for each tree ring (*cf*. Hereş *et al*., 2014). To assign the correct calendar year to all these variables, the tree-ring series were visually cross-dated among trees and compared with published site ring-width chronologies (Camarero *et al*., 2015). In total, 475 673 and 976 510 tracheids were measured in Scots pine and silver fir, respectively, considering the 1950–2012 period (1 214 725 and 1 409 018 tracheids considering the whole chronologies).

The parenchyma rays were measured across tangential sections in six trees per species to obtain a proxy for potential storage of nonstructural carbohydrates in the wood (*cf*. Olano *et al*., 2013; von Arx *et al*., 2015). We summed the area covered by parenchyma cells across a 4-mm^2 tangential surface, paying attention to not consider the area of resin canals. Since parenchyma rays generally extend through several tree rings (3 on average), we cut tangential sections every five rings and computed the mean parenchyma area every 10 years.

Water-use efficiency inferred from carbon isotope discrimination

To compare the changes in iWUE of nondeclining and declining trees we measured $^{13}C/^{12}C$ isotope ratios in the stem wood. We used the same trees selected for wood-anatomical analyses and with a razor blade under a binocular microscope we carefully separated decadal wood segments for the period 1900–2010. We preferred this time resolution to account for a sufficient number of trees while keeping the low-frequency variability as for the parenchyma rays measurements.

Wood samples were homogenized and milled using an ultra-centrifugation mill (Retsch ZM1). An aliquot of 0.5 mg of each wood sample was weighed on a balance (Mettler

Toledo AX205) and placed into a tin capsule for isotopic analyses. Cellulose was not extracted, since both whole wood and cellulose isotope time-series showed similar long-term trends related to atmospheric CO_2 concentration and climate (Saurer *et al.*, 2004). Furthermore, a carryover effect from year to year can be regarded as negligible, given that we analysed decades. The isotope ratio $^{13}C/^{12}C$ ($\delta^{13}C$) was determined on an isotope ratio mass spectrometer (ThermoFinnigan MAT 251) at the Stable Isotope Facility (University of California, Davis, USA). The results were expressed as relative differences in the $^{13}C/^{12}C$ ratio of tree material with respect to the Vienna Pee-Dee Belemnite (V-PDB) standard. The accuracy and precision of analyses were 0.07‰ and ±0.1‰, respectively.

Isotopic discrimination between the carbon of atmospheric CO_2 and wood carbon (Δ; see Farquhar & Richards, 1984) was defined as:

$$\Delta = (\delta^{13}C_{air} - \delta^{13}C_{plant})/(1 + \delta^{13}C_{plant}/1000), \quad (1)$$

where $\delta^{13}C_{air}$ and $\delta^{13}C_{plant}$ are the isotope ratios of carbon ($^{13}C/^{12}C$) in atmospheric CO_2 and tree-ring wood, respectively, expressed in parts per thousand (‰) relative to the standard V-PDB; Δ is linearly related to the ratio of intercellular (c_i) to atmospheric (c_a) CO_2 mole fractions, by:

$$\Delta = a + (b - a)c_i/c_a, \quad (2)$$

where a is the fractionation during CO_2 diffusion through the stomata (4.4‰), and b is the fractionation associated to Rubisco and other enzymes (Farquhar & Richards, 1984). The values of c_a and $\delta^{13}C_{air}$ were obtained from McCarroll & Loader (2004) and from Mauna Loa (Hawaii) records.

The c_i/c_a ratio reflects the balance between net assimilation (A) and stomatal conductance for CO_2 (g_c) according to Fick's law: $A = g_c(c_a - c_i)$. Stomatal conductances for CO_2 and water vapour (g_w) are related by a constant factor ($g_w = 1.6g_c$), and hence these last two variables allow linking the leaf-gas exchange of carbon and water. The linear relationship between c_i/c_a and Δ may be used to calculate the iWUE (μmol mol^{-1}) as:

$$\text{iWUE} = (c_a/1.6)[(b - \Delta)/(b - a)] \quad (3)$$

Statistical analyses

We used Generalized Additive Models (GAM; Wood, 2006) to study within- and between year variability in lumen area of declining and nondeclining trees. GAMs are a semiparametric case of generalized linear models in which the response variable depends on a collection of smooth functions of the explanatory variable (Hastie & Tibshirani, 1990). Thus, they represent a flexible method to characterize nonlinear trends in time-series that vary at different temporal scales, such as wood-anatomical data. Since tree rings reflect the variability of lumen area anatomy between (long-term) and within (short-term) years we proposed a GAM that includes two different smooth terms: one reflecting between-years variability and another corresponding to the within-year variability in lumen area summarized as a continuous variable that ranges from 0 (early earlywood, beginning of the ring) to 100 (late latewood, end of the ring) indicating how lumen area changes along the relative position within each ring (*cf*. Cuny *et al*., 2014). For each species (silver fir and Scots pine) and vigour class (declining vs nondeclining trees), we obtained the mean lumen areas along the first 60% of each ring, that is the three earlywood sectors which account for most (around 90%) of the K_h of the whole ring. These series were obtained for the 1950–2012 period and they were used as response variables in the subsequent analyses.

The GAM proposed had the form:

$$\text{Lumen area}_i = s(\text{within year trend}_i) + s(\text{between years trend}_i) + e_i \quad (4)$$

In which the lumen area of a ring i of declining and nondeclining trees is modelled as smooth functions (s) of the within- and between-years trends. The smooth terms were represented using default settings of the function *gamm* in the *mgcv* package (Wood, 2006) of the R environment (R Development Core Team, 2014).

To study the influence of vigour class and climate on cell size formation we used a multi-model inference approach based on information theory (Burnham & Anderson, 2002). This approach relies on the use of information theory to calculate the probability that a given model is more appropriate than other competing models to explain the response variable. We proposed 10 models including vigour class and selected climatic variables and their interactions with the two smooth terms (see Table S1). Climatic variables were first of all analysed through Pearson's correlation with the response variables (tracheid features) and we then selected the strongest correlations. We ranked all the potential models that could be generated with the different explanatory variables according to the second-order Akaike Information Criterion (AICc). For each model, we calculated its ΔAICc, i.e. the difference between AICc of each model and the minimum AICc found for the set of fitted models. The ΔAICc can be used to select those models that best explain the response variable since values of ΔAICc lower than two indicate that the considered model is as good a candidate as the best model. Carbon-isotope data were analysed using linear mixed-effects models considering tree vigour (declining vs nondeclining trees) and time (decades) as fixed factors. The MuMIn package (Barton, 2012) of the R environment (R Development Core Team, 2014) was used to perform the multimodel selection. Finally, to compare declining vs nondeclining trees without considering the time dimension, we adopted the Mann–Whitney test, a nonparametric method used to contrast two groups without considering any distribution information on the population (Sokal & Rohlf, 2012).

Results

Declining and nondeclining trees did not differ significantly in terms of diameter, height, age or neighbourhood basal area (one-way ANOVAs, $F = 2.80–0.51$, $P = 0.12–0.49$; Table 1).

However, declining trees of both species had narrower rings formed by fewer tracheids than nondeclining trees.

Table 1 Structural variables describing nondeclining and declining Scots pine and silver fir trees. Data are means ± SE

	Scots pine		Silver fir	
	Nondeclining trees	Declining trees	Nondeclining trees	Declining trees
No. trees	5	5	5	5
Diameter at 1.3 m (cm)	25.1 ± 3.2	26.7 ± 2.0	38.5 ± 3.7	32.0 ± 3.0
Tree height (m)	8.7 ± 1.2	8.4 ± 1.0	25.4 ± 1.8	22.5 ± 1.8
Age (years)	136 ± 17	137 ± 9	98 ± 8	90 ± 10
Neighbourhood basal area (m^2 ha^{-1})	10.8 ± 2.0	7.8 ± 1.0	20.4 ± 5.3	14.3 ± 2.8
Crown cover (%)	75 ± 6 b	15 ± 5 a	96 ± 2 b	35 ± 4 a

Different letters indicate significantly different values ($P < 0.05$) based on Mann–Whitney test.

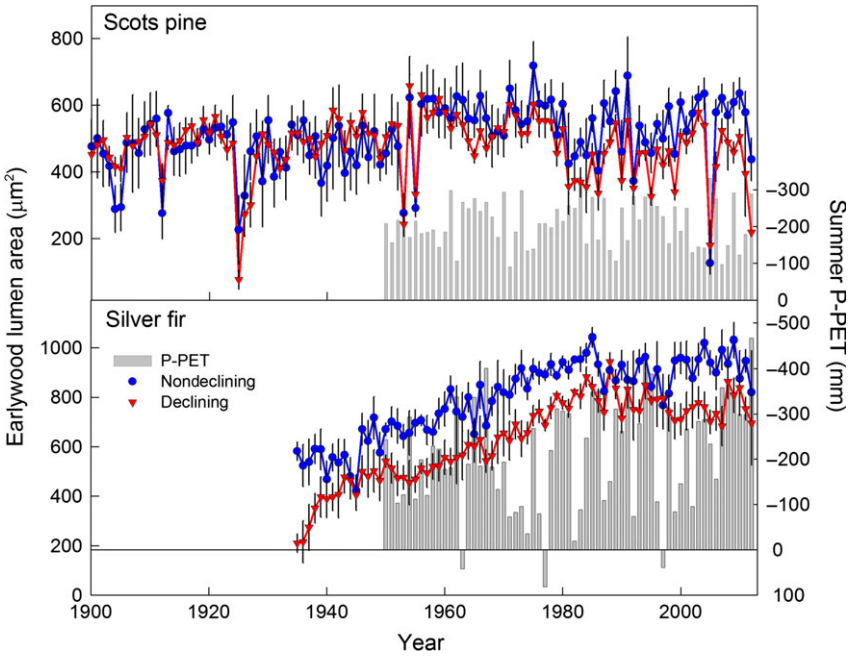

Fig. 1 Annual values of earlywood lumen area in nondeclining and declining trees of Scots pine and silver fir as related to spring or summer water balance (P-PET), respectively (the bars and right y-axis correspond to the water balance; note the reverse scales). Wood anatomy data are means ± SE.

In addition, earlywood tracheids in nondeclining trees had larger lumen areas and thinner cell walls. Consequently, the theoretical earlywood K_h of declining trees decreased while their $(CWT/LD)^2$ increased (Fig. 1 and Table 2; see also Fig. S3).

Wet conditions during the growing season promoted larger lumen in earlywood tracheids while lumen area sharply dropped during dry years (2005, 2012) in the case of Scots pine (Fig. 1). In this species we also noticed reductions in earlywood lumen area, more pronounced in declining trees, during years without dry springs such as 1953 and 1955 and during years without available climate data such as 1925. In silver fir, earlywood lumen area increased steadily from the 1930s to about 1985 at a mean rate of 9.5 μm^2 yr^{-1}. These significant and positive trends did not significantly differ between nondeclining and declining trees ($F = 1.90$, $P = 0.17$). Lumen area in both tree groups was then abruptly reduced after the dry summer in 1985, reaching similar values (ca. 900 μm^2) in 1988. Instead, declining Scots pine trees presented a significant ($P = 0.003$) reduction in lumen area since 1950 at a mean rate of -2.0 μm^2 yr^{-1}, whereas nondeclining trees did not, i.e. there was a long-term divergence between the two vigour classes (significant time x vigour interaction, $F = 7.86$, $P = 0.005$).

Overall, wood anatomy traits responded more to yearly climate variability among Scots pines than in silver firs, with minor differences being observed between the vigour classes. The spring and summer

Table 2 Statistics describing the mean values of measured and derived wood-anatomical variables of nondeclining (ND) and declining (D) Scots pine and silver fir trees

	Scots pine				Silver fir			
	Earlywood		Latewood		Earlywood		Latewood	
	ND	D	ND	D	ND	D	ND	D
Lumen area (μm^2)	542.6 ± 17.2 b	471.8 ± 17.8 a	141.5 ± 8.8	126.3 ± 7.5	850.3 ± 20.2 b	684.9 ± 20.0 a	128.0 ± 6.3	100.54 ± 5.95
Cell-wall thickness (μm)	3.86 ± 0.04 a	4.08 ± 0.06 b	4.98 ± 0.10	5.11 ± 0.11	3.71 ± 0.06 a	3.93 ± 0.06 b	6.60 ± 0.07	6.73 ± 0.06
K_h (kg m MPa^{-1} s^{-1}) 10^{-15}	1.22 ± 0.05 b	0.97 ± 0.04 a	0.18 ± 0.02	0.15 ± 0.01	2.30 ± 0.08 b	1.69 ± 0.07 a	0.14 ± 0.02	0.11 ± 0.01
C_{cost} (μm)	1458.8 ± 100.8	1753.6 ± 236.0	1040.9 ± 77.0	1108.0 ± 90.8	3244.7 ± 239.1	3485.8 ± 243.1	3138.7 ± 225.5	2907.0 ± 185.8
$(CWT/LD)^2$	0.11 ± 0.01 a	0.14 ± 0.01 b	0.71 ± 0.06	0.82 ± 0.08	0.06 ± 0.01 a	0.09 ± 0.01 b	1.19 ± 0.06	1.25 ± 0.08

	Tree ring			
	ND (n = 193 661 tracheids)	D (n = 282 012 tracheids)	ND (n = 544 015 tracheids)	D (n = 43 2495 tracheids)
No. tracheids	655 ± 20 b	525 ± 21 a	1508 ± 51 b	1168 ± 40 a
Width (μm)	645.9 ± 47.1 b	539.2 ± 51.3 a	2109.1 ± 115.0 b	1583.3 ± 111.5 a
Ray parenchyma area (μm^2)	94.6 ± 4.7	90.0 ± 6.6	61.8 ± 2.5	58.9 ± 1.9

Values are presented separately for earlywood and latewood or for the whole tree-ring (last two lines; n is the number of measured tracheids). Data are means ± SE and correspond to the 1950–2012 period. Different letters indicate significant ($P < 0.05$) differences based on Mann–Whitney tests. Abbreviations of variables are: K_h, theoretical hydraulic conductivity; C_{cost}, carbon cost of tracheid formation; CWT/LD, cell-wall thickness-to-span ratio.

water balances were the major climatic drivers of Scots pine and silver fir earlywood lumen areas, respectively (Fig. S4). Differences in lumen area were more evident during wet than dry years (Fig. S5). A previous wet winter and cold and wet summer conditions enhanced the formation of thicker latewood tracheids in Scots pine, whereas warm summer conditions did in silver fir.

We found no significant differences in parenchyma area between tree vigour classes (Table 2, Fig. 2). Only in the last decade (2000s) nondeclining trees tended to produce more parenchyma area than declining ones (Fig. 2), but differences were not significant (Scots pine, $P = 0.35$; silver fir, $P = 0.42$).

According to the fitted GAMs, the climatic signal of lumen area was stronger in Scots pine, whereas the interaction between climate and tree vigour was stronger in silver fir (Table 3, Fig. 3). The GAMs accounted for 79% and 95% of the lumen area variation in Scots pine and silver fir, respectively (Table 3; see also Table S1). These models confirmed that the lumen areas in declining and nondeclining trees had diverged at least since the 1950s with a slight trend to convergence in the late 1980s only in the case of silver fir. The within-ring pattern of lumen area variability was very similar between vigour classes, with differences magnified just in the early to mid earlywood where tracheids reached the largest size.

In Scots pine, declining trees presented significantly ($F = 81.6$, $P < 0.001$) higher $\delta^{13}C$ values (mean ± SD = −23.5 ± 0.2 ‰) than nondeclining trees (−24.3 ± 0.3 ‰) (Fig. 4). However, in silver fir we found the opposite pattern (declining trees, −25.6 ± 0.4 ‰; nondeclining trees, −24.9 ± 0.7 ‰) and differences were again significant albeit less marked ($F = 7.8$, $P = 0.01$). In both species $\delta^{13}C$ values significantly decreased along time (Scots pine, $F = 5.6$, $P = 0.03$; silver fir, $F = 6.9$, $P = 0.02$). No significant decline x time interactions were detected, but declining and nondeclining Silver firs presented similar $\delta^{13}C$ values from the 1990s onwards, whereas a significant negative trend in $\delta^{13}C$ was only detected in nondeclining Scots pine trees (slope = −0.006, $P = 0.015$). Accordingly, only nondeclining Scots pine trees presented a sustained increase in iWUE, particularly since the 1980s (Fig. 4). In agreement with $\delta^{13}C$ values, declining silver firs presented a lower mean iWUE (73 μmol mol^{-1}) than nondeclining trees (81 μmol mol^{-1}), but this difference disappeared in the 1990s. However, a reverse pattern was observed in Scots pine with declining trees showing higher iWUE (92 μmol mol^{-1}) than nondeclining ones (84 μmol mol^{-1}) and this divergence was more marked since the 1960s.

Discussion

Our findings confirm that declining trees were prone to drought-induced dieback because they produced smaller lumen areas which potentially provide less hydraulic conductivity to trees and constrain their ability to grow. Such anatomic and hydraulic divergence with respect to the nondeclining trees could be considered a predisposing factor (*sensu* Manion, 1991) since it was detected several decades (1950s in Scots pine, at least since the 1980s in silver fir) before the droughts

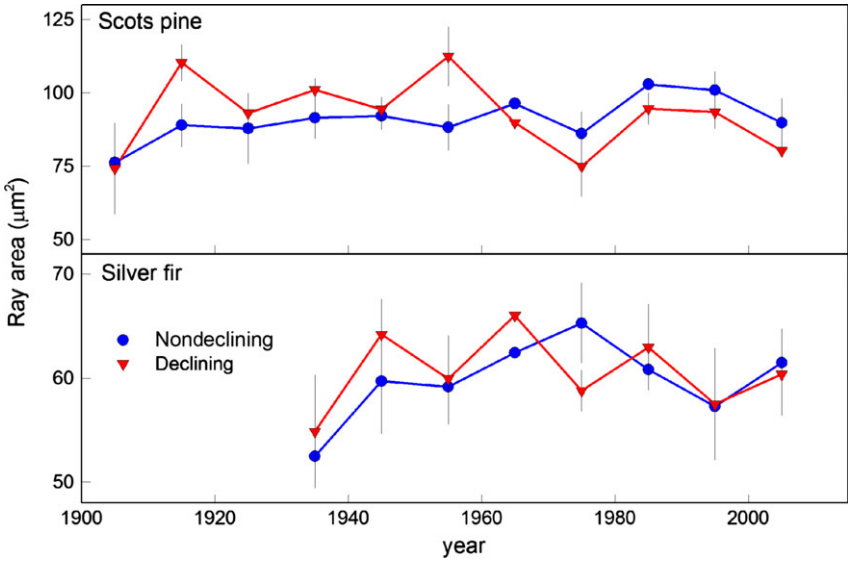

Fig. 2 Decadal variability in the parenchyma ray area of nondeclining and declining trees of Scots pine and silver fir. Values are means ± SE.

Table 3 Statistics corresponding to generalized additive models of earlywood lumen area (*edf*, degrees of freedom; *F* value; *P*, probability level)

Species	Factors	*edf*	*F*	*P*
Scots pine	Long-term trend			
	*vigour: nondeclining	8.88	76.5	<0.001
	*vigour: declining	8.88	71.8	<0.001
	Short-term trend			
	*vigour: nondeclining	8.89	2556.2	<0.001
	*vigour: declining	8.86	2358.3	<0.001
	Climate (P-ETP)	1	930.2	<0.001
	*vigour	1	4.1	0.042
	vigour	1	17.2	<0.001
Silver fir	Long-term trend			
	*vigour: nondeclining	8.79	199.8	<0.001
	*vigour: declining	8.43	632.0	<0.001
	Short-term trend			
	*vigour: nondeclining	8.91	12423	<0.001
	*vigour: declining	8.94	12407	<0.001
	Climate (P-ETP)	1	4.07	0.003
	*vigour	1	24.16	<0.001
	vigour	1	1461.02	<0.001

These models described the long-term and short-term trends of lumen area, i.e. the interannual and intra-annual variability, respectively, as related to tree vigour (declining vs nondeclining trees) and seasonal water balance (P-PET; spring and summer water balances were considered for Scots pine and silver fir, respectively). We created a model containing a continuous variable representing the long-term trend (between rings) in wood anatomy and a variable ranging from 0 to 100 (relative tree-ring width) showing the short-term (within rings) lumen area trend for each species (Scots pine, silver fir). The short-term and long-term terms of lumen area were modelled as thin plate regression splines, whereas the effect of climate was regarded as linear.

triggered die-off and induced mortality (Figs 1 and 3). Short-term investigations have shown that the reduction in hydraulic conductivity can be counterbalanced by concurrent changes in sapwood and leaf area allowing a similar capacity to supply leaves with water (Hereş *et al*., 2014). However, tuning the leaf-to-sapwood area ratio does not seem an adequate and valid strategy to fully offset the long-term reduction of lumen area detected in declining trees. Yet, the reconstruction of wood-anatomical variables supports die-off mechanisms related to enduring hydraulic deterioration, and it is much less consistent with those concerning carbon starvation. Although the process of tree death is complex and involves a suite of parallel declines throughout multiple tissues (Anderegg *et al*., 2014), we have contributed solid evidence confirming that long-term and plastic adaptations in xylem traits such as lumen area do allow identifying trees vulnerable to drought stress in terms of growth decline and vigour loss.

This long-term predisposing factor is also confirmed at functional level with the clear separation in iWUE between trees of different vigour. Here, the reverse pattern observed between the species could be explained by the idiosyncratic drought sensitivity of the species with silver fir being much more drought-sensitive respect to the 'drought-avoiding' Scots pine (Irvine *et al*., 1998; Aussenac, 2002). In addition, the higher iWUE of declining Scots pine trees could indicate that they experience long-term drier local conditions due to particular soil characteristics (lower soil water holding capacity), or because they form shallow root systems. Nevertheless, the lower iWUE of declining silver firs as compared with nondeclining conspecifics and the convergence from the 1990s onwards suggest that both tree vigour classes are becoming less able to regulate their water loss in response to warming-induced evapotranspiration deficits (Vicente-Serrano *et al*., 2015). Overall, carbon-isotope data produced opposite patterns in two tree species experiencing dieback which indicate that iWUE reconstructions should be always supported by additional long-term datasets of tree functioning such as growth, changes in leaf and sapwood area, and wood-anatomical data.

Wet conditions during the growing season promoted the formation of larger lumen areas and thus increased the theoretical hydraulic conductivity of tracheids. However, nondeclining trees seemed more prompt than declining ones to enlarge lumen area in response to higher water availability, particularly in the case of Scots pine. The divergence in this species can be traced back to the 1950s, suggesting a long-term deterioration in hydraulic conductivity. Drought stress, i.e. evaporative demand that is not met by available water (*cf*. Stephenson, 1998), is mainly controlled by air temperatures at the Scots pine site, which is drier than the silver fir one. Wood-anatomical data, echoed by growth data (Camarero *et al*., 2015), together with the higher responsiveness to climate detected in the Scots pine site as compared with the silver fir site confirmed this. We must also emphasize that the Scots pine stand constitutes one of the southernmost and drought-exposed limits of distribution of the species.

The two conifers also presented seasonal differences in the wood anatomical responses to climate with spring or summer water balance controlling earlywood lumen area and conductivity in Scots pine, whilst in silver fir previous summer water balance was the most relevant driver of lumen area (Table 3) and also of radial growth (Camarero *et al*., 2011). The different climatic drivers of wood formation are further illustrated by the contrasting conditions enhancing latewood cell-wall thickening which, during late xylogenesis (summer growing season), was more related to water

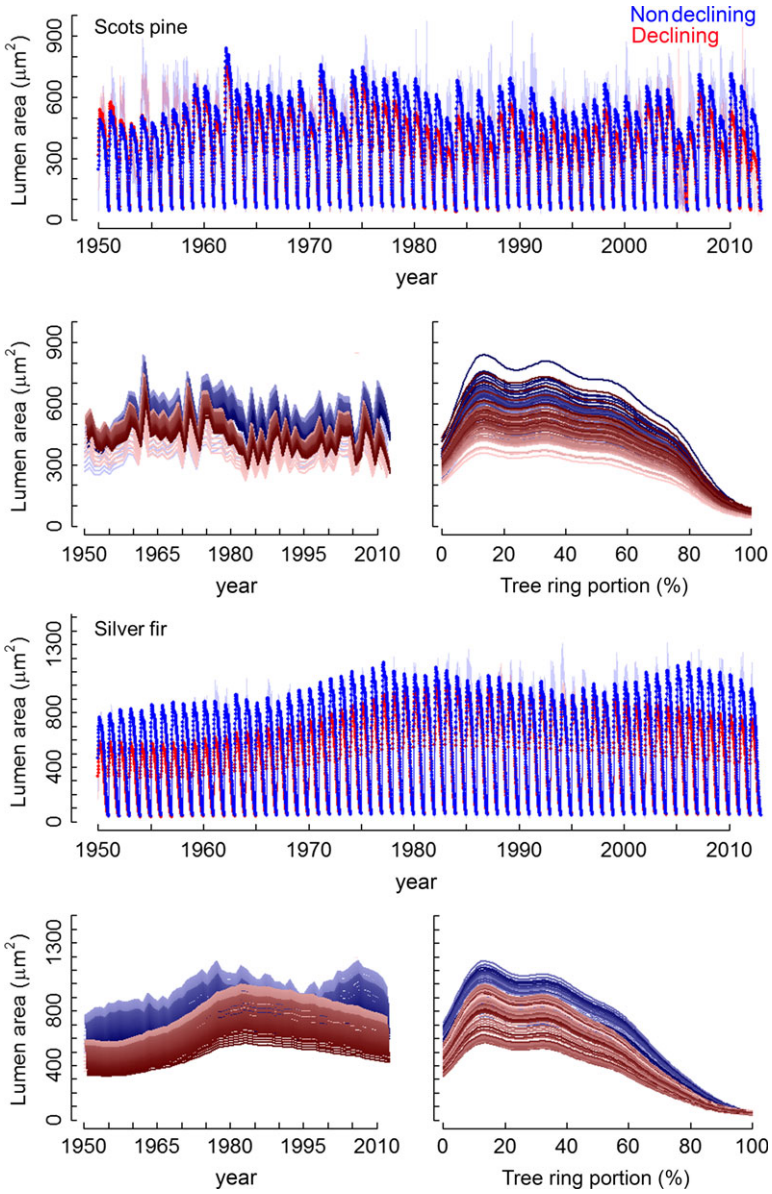

Fig. 3 Observed (thin lines) and modelled long- (between annual ring) and short-term (within a ring) fitted trends in lumen area of nondeclining and declining in Scots pine and silver fir. Generalized additive models were used to characterize the changes in lumen area. These changes are plotted (i) by comparing between years (first 60% portion of the ring; lines of darker and lighter colours corresponding to firstly and lastly formed tracheids, respectively, lower plots to the left); and (ii) by describing lumen area within a ring (darker and lighter colours corresponding to wetter and drier conditions, respectively; note that the differences are more marked in the Scots pine than in the silver fir).

availability in Scots pine and to temperature in silver fir.

The wood-anatomical traits considered did not indicate that declining and nondeclining trees presented different xylem resistances against embolism, although the $(CWT/LD)^2$ ratio may not fully reflect the actual xylem vulnerability to embolism (Domec *et al.*, 2006; Choat *et al.*, 2008; Hacke & Jansen, 2009), More importantly, none of the measured (parenchyma area) or calculated (C_{cost}) variables support the hypothesis that declining trees were presenting previous or concurrent symptoms of carbon starvation as evaluated in the stem wood. Carbon starvation is a highly complex process and the anatomical proxies we considered may not permit to fully assess the processes involved in carbon fixation and use within a tree. However, our findings are consistent with the slight predrought decreases in the concentrations of sapwood soluble sugars in the

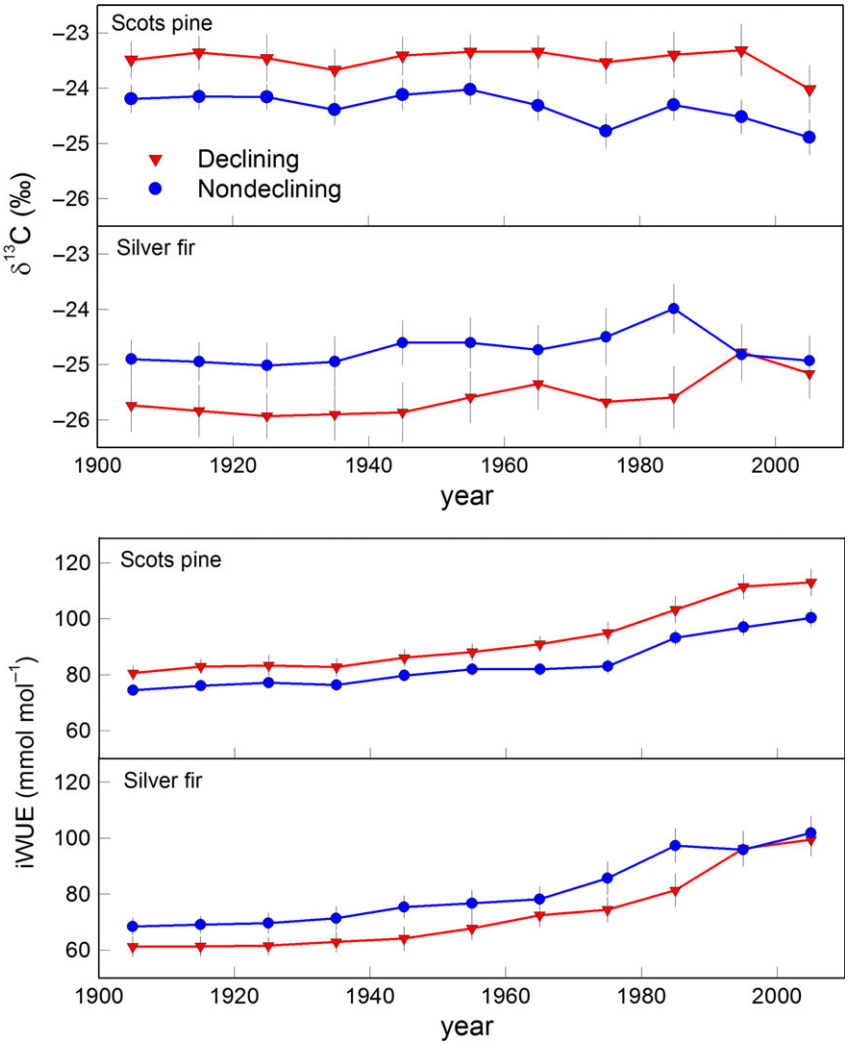

Fig. 4 Trends of wood carbon-isotope discrimination ($\delta^{13}C$) and intrinsic water-use efficiency (iWUE) of declining and nondeclining silver firs and Scots pines. Values are means ± SE.

declining and most defoliated trees of both species during 2012, which were followed by postdrought increases in the case of silver fir (Camarero *et al.*, 2015). We interpret these changes as responses to drought-induced declines in sink activity such as wood formation or to the formation of mobile sugars refilling embolized tracheids (Dietze *et al.*, 2014). Furthermore, declining silver firs presented a lower physiological performance than nondeclining trees confirming that late-summer drought (elevated vapour pressure deficit due to high evapotranspiration rates) caused die-off in the mesic silver-fir site (Peguero-Pina *et al.*, 2007).

In the case of silver fir the increase in earlywood lumen area from the 1930s to the mid-1980s agrees with the typical ontogenetic trend, manifested regardless of the vigour status, and linked to height growth (Carrer *et al.*, 2015). This suggests that silver firs were steadily increasing their hydraulic conductivity and growth capacity until the late-summer 1985 drought caused a sharp decline in earlywood area of all trees, preceding the die-off observed in the 2010s (Fig. 1). It was during the 1980s when lumen areas of declining and nondeclining trees almost converged (Figs 1 and 3), as in fact occurred with iWUE in sites showing high and low dieback intensity (Linares & Camarero, 2012). From the 1980s onwards, these authors reported a progressive drought-induced growth decline and a reduced iWUE improvement in declining silver firs, which they interpreted as reflecting a constant ratio between intercellular and atmospheric CO_2 concentrations. This study confirms that declining silver firs consistently produced smaller lumens and thus always showed lower hydraulic conductivity than nondeclining trees. In other words, declining silver firs were more prone to

drought-induced dieback due to their inferior hydraulic and radial-growth performances as compared with nondeclining trees. The loss in hydraulic performance translated into growth decline (Camarero *et al*., 2015), and possibly reduced photosynthetic rates, could be linked to the low stomatal control of leaf gas exchange in silver fir in response to warming-induced vapour pressure deficits (Aussenac, 2002). Furthermore, our findings confirm that the rise in atmospheric CO_2, aligned with the corresponding increase in iWUE, did not counterbalance the negative effects of droughts on growth and conductivity, whose decreases were the final drivers of the die-off. For both Scots pine and silver fir, the hydraulic deterioration prior to the die-off could be considered a chronic process since the water balance has been steadily decreasing from the 1950s onwards in both study areas. In addition, the declining trees showed similar diameter respect to nondeclining trees, but lower cells dimension, and this suggests that declining trees were larger than nondeclining before the dieback process started. This assumption may be explained by the fact that big trees are differently coupled with the environment than smaller trees.

It is evident that this study raises many questions related to the ultimate causes making trees more susceptible to decline in hydraulic terms. Ongoing research will investigate if soils or microtopographic features determine the different susceptibility of neighbouring trees to drought stress, particularly in the case of Scots pine. Genetic predisposition to drought-induced die-off within a tree population is also an unknown driver, albeit it has been proved that genetic variability between populations is related to their susceptibility to dieback in the case of silver fir (Sancho-Knapik *et al*., 2014). Lastly, environmental and genetic drivers could also interact determining tree vigour and vulnerability to drought.

To conclude, this research evidences that long-lasting wood-anatomical differences prior to the onset of water shortage predispose trees to selective drought-induced dieback. Declining trees of both Scots pine and silver fir were those least fit from the hydraulic point of view. In Scots pine the divergence between declining and nondeclining trees can be traced back to fifty years prior to the die-off, whilst in silver fir the tracheid-lumen areas of declining trees were consistently and significantly smaller during the whole ontogeny, and therefore they presented a lower hydraulic performance. None of the analysed wood-anatomical variables supported carbon starvation as a major mechanism of the present die-off phenomena. Retrospective analyses of lumen-area time series could be used as prognosis tools to predict which trees are more prone to drought-induced die-off. Improving these forecasts by increasing the number of trees, sites and species under investigation is urgent since many conifer stands will be more widely affected by drought-induced die-offs in the Anthropocene (Allen *et al*. 2015; Anderegg *et al*., 2015).

Acknowledgements

This study was supported by projects 387/2011 (OAPN, Spanish Ministry of Environment) and CGL2011-26654 (Spanish Ministry of Economy). We thank the FPS COST Action FP1106 STReESS for facilitating collaborative work. We acknowledge AEMET for providing climatic data. A. Gazol is supported by a Postdoctoral grant from MINECO (Contrato Formacion Postdoctoral MINECO - FPDI 2013-16600, FEDER funds).

References

Allen CD, Macalady AK, Chenchouni H *et al*. (2010) A global overview of drought and heat-induced tree mortality reveals emerging climate change risks for forests. *Forest Ecology and Management*, **259**, 660–684.

Anderegg WRL (2015) Spatial and temporal variation in plant hydraulic traits and their relevance for climate change impacts on vegetation. *New Phytologist*, **205**, 1008–1014.

Anderegg WRL, Plavcová L, Anderegg LDL, Hacke UG, Berry JA, Field CB (2013) Drought's legacy: multiyear hydraulic deterioration underlies widespread aspen forest die-off and portends increased future risk. *Global Change Biology*, **19**, 1188–1196.

Anderegg WRL, Anderegg LDL, Berry JA, Field CB (2014) Loss of whole-tree hydraulic conductance during severe drought and multi-year forest die-off. *Oecologia*, **175**, 11–23.

Anderegg WRL, Schwalm C, Biondi F *et al*. (2015) Pervasive drought legacies in forest ecosystems and their implications for carbon cycle models. *Science*, **349**, 528–532.

von Arx G, Carrer M (2014) ROXAS – A new tool to build centuries-long tracheid-lumen chronologies in conifers. *Dendrochronologia*, **32**, 290–293.

von Arx G, Arzac A, Olano JM, Fonti P (2015) Assessing conifer ray parenchyma for ecological studies: pitfalls and guidelines. *Frontiers in Plant Science*, **6**, 1016.

Aussenac G (2002) Ecology and ecophysiology of circum-Mediterranean firs in the context of climate change. *Annals of Forest Science*, **59**, 823–832.

Babst F, Bouriaud O, Papale D *et al*. (2014) Above-ground woody carbon sequestration measured from tree rings is coherent with net ecosystem productivity at five eddy-covariance sites. *New Phytologist*, **201**, 1289–1303.

Barton K (2012) MuMIn: multi-model inference. R package, version 0.12.2.

Bonan GB (2008) Forests and climate change: forcings, feedbacks, and the climate benefits of forests. *Science (New York, N.Y.)*, **320**, 1444–1449.

Bréda N, Huc R, Granier A, Dreyer E (2006) Temperate forest trees and stands under severe drought: a review of ecophysiological responses, adaptation processes and long-term consequences. *Annals of Forest Science*, **63**, 625–644.

Bryukhanova M, Fonti P (2013) Xylem plasticity allows rapid hydraulic adjustment to annual climatic variability. *Trees - Structure and Function*, **27**, 485–496.

Burnham KP, Anderson DR (2002) *Model Selection and Multimodel Inference: a Practical Information-theoretic Approach*, 2nd edn, Vol. 60. Springer-Verlag, New York, NY.

Camarero JJ, Bigler C, Linares JC, Gil-Pelegrín E (2011) Synergistic effects of past historical logging and drought on the decline of Pyrenean silver fir forests. *Forest Ecology and Management*, **262**, 759–769.

Camarero JJ, Gazol A, Sangüesa-Barreda G, Oliva J, Vicente-Serrano SM (2015) To die or not to die: early warnings of tree dieback in response to a severe drought. *Journal of Ecology*, **103**, 44–57.

Carrer M, Von ArxG, Castagneri D, Petit G (2015) Distilling allometric and environmental information from time series of conduit size: the standardization issue and its relationship to tree hydraulic architecture. *Tree Physiology*, **35**, 27–33.

Choat B, Cobb AR, Jansen S (2008) Structure and function of bordered pits: new discoveries and impacts on whole-plant hydraulic function. *New Phytologist*, **177**, 608–626.

Cuny HE, Rathgeber CBK, Frank D, Fonti P, Fournier M (2014) Kinetics of tracheid development explain conifer tree-ring structure. *New Phytologist*, **203**, 1231–1241.

Denne M (1988) Definition of latewood according to Mork. *Iawa Bull*, **10**, 59–62.

Dietze MC, Sala A, Carbone MS, Czimczik CI, Mantooth JA, Richardson AD, Vargas R (2014) Nonstructural carbon in woody plants. *Annual Review of Plant Biology*, **65**, 667–687.

Dobbertin M (2005) Tree growth as indicator of tree vitality and of tree reaction to environmental stress: a review. *European Journal of Forest Research*, **124**, 319–333.

Domec JC, Lachenbruch B, Meinzer FC (2006) Bordered pit structure and function determine spatial patterns of air-seeding thresholds in xylem of douglas-fir (*Pseudotsuga menziesii*; Pinaceae) trees. *American Journal of Botany*, **93**, 1588–1600.

Eilmann B, Zweifel R, Buchmann N, Fonti P, Rigling A (2009) Drought-induced adaptation of the xylem in Scots pine and pubescent oak. *Tree Physiology*, **29**, 1011–1020.

Eilmann B, Zweifel R, Buchmann N, Graf Pannatier E, Rigling A (2011) Drought alters timing, quantity, and quality of wood formation in Scots pine. *Journal of Experimental Botany*, **62**, 2763–2771.

Farquhar GD, Richards RA (1984) Isotopic composition of plant carbon correlates with water-use efficiency of wheat genotypes. *Australian Journal of Plant Physiology*, **11**, 539–552.

Fonti P, Von Arx G, García-González I, Eilmann B, Sass-Klaassen U, Gärtner H, Eckstein D (2010) Studying global change through investigation of the plastic responses of xylem anatomy in tree rings. *New Phytologist*, **185**, 42–53.

Galiano L, Martínez-Vilalta J, Lloret F (2011) Carbon reserves and canopy defoliation determine the recovery of Scots pine 4 yr after a drought episode. *New Phytologist*, **190**, 750–759.

Gutschick VP, BassiriRad H (2003) Extreme events as shaping physiology, ecology, and evolution of plants: toward a unified definition and evaluation of their consequences. *New Phytologist*, **160**, 21–42.

Hacke UG, Jansen S (2009) Embolism resistance of three boreal conifer species varies with pit structure. *New Phytologist*, **182**, 675–686.

Hacke UG, Sperry JS, Pockman WT, Davis SD, McCulloh KA (2001) Trends in wood density and structure are linked to prevention of xylem implosion by negative pressure. *Oecologia*, **126**, 457–461.

Hastie TJ, Tibshirani R (1990) *Generalized Additive Models*, vol. 1, pp. 297–318. Chapman & Hall, New york, NY, USA.

Hereş A-M, Camarero J, López B, Martínez-Vilalta J (2014) Declining hydraulic performances and low carbon investments in tree rings predate Scots pine drought-induced mortality. *Trees*, **28**, 1737–1750.

Hoffmann WA, Marchin RM, Abit P, Lau OL (2011) Hydraulic failure and tree dieback are associated with high wood density in a temperate forest under extreme drought. *Global Change Biology*, **17**, 2731–2742.

Hsiao T (1973) Plant responses to water stress. *Annual review of Plant Physiology*, **24**, 519–570.

Irvine J, Perks MP, Magnani F, Grace J (1998) The response of Pinus sylvestris to drought: stomatal control of transpiration and hydraulic conductance. *Tree Physiology*, **18**, 393–402.

IPCC (2014) Climate change 2014: impacts, adaptation, and vulnerability. In: *Part B: Regional Aspects. Contribution of Working Group II to the Fifth Assessment Report of the Intergovernmental Panel on Climate Change*, (eds Barros VR, Field CB, Dokken DJ, Mastrandre MD, Mach KJ, Bilir TE, Chatterjee M, Ebi KL, Estrada YO, Genova RC, Girma B, Kissel ES, Levy AN, MacCracken S, Mastrandrea PR, White LL), Cambridge University Press, Cambridge.

Klein T (2014) The variability of stomatal sensitivity to leaf water potential across tree species indicates a continuum between isohydric and anisohydric behaviours. *Functional Ecology*, **28**, 1313–1320.

Knapic S, Pereira H (2005) Within-tree variation of heartwood and ring width in maritime pine (*Pinus pinaster* Ait.). *Forest Ecology and Management*, **210**, 81–89.

Körner C (2003) Carbon limitation in trees. *Journal of Ecology*, **91**, 4–17.

Levanič T, Čater M, McDowell NG (2011) Associations between growth, wood anatomy, carbon isotope discrimination and mortality in a Quercus robur forest. *Tree Physiology*, **31**, 298–308.

Lévesque M, Saurer M, Siegwolf R, Eilmann B, Brang P, Bugmann H, Rigling A (2013) Drought response of five conifer species under contrasting water availability suggests high vulnerability of Norway spruce and European larch. *Global Change Biology*, **19**, 3184–3199.

Liang W, Heinrich I, Simard S, Helle G, Liñán ID, Heinken T (2013) Climate signals derived from cell anatomy of scots pine in NE Germany. *Tree Physiology*, **33**, 833–844.

Linares JC, Camarero JJ (2012) From pattern to process: linking intrinsic water-use efficiency to drought-induced forest decline. *Global Change Biology*, **18**, 1000–1015.

Manion PD (1991) *Tree Disease Concepts*. Prentice Hall, Englewood Cliffs, NJ, USA.

Martin-Benito D, Beeckman H, Cañellas I (2013) Influence of drought on tree rings and tracheid features of *Pinus nigra* and *Pinus sylvestris* in a mesic Mediterranean forest. *European Journal of Forest Research*, **132**, 33–45.

McCarroll D, Loader NJ (2004) Stable isotopes in tree rings. *Quaternary Science Reviews*, **23**, 771–801.

McDowell NG (2011) Mechanisms linking drought, hydraulics, carbon metabolism, and vegetation mortality. *Plant Physiology*, **155**, 1051–1059.

McDowell N, Pockman WT, Allen CD *et al.* (2008) Mechanisms of plant survival and mortality during drought: why do some plants survive while others succumb to drought? *New Phytologist*, **178**, 719–739.

Olano JM, Arzac A, Garcia-Cervigon AI, Von Arx G, Rozas V (2013) New star on the stage: amount of ray parenchyma in tree rings shows a link to climate. *New Phytologist*, **198**, 486–495.

Pacheco A, Camarero J, Carrer M (2015) Linking wood anatomy and xylogenesis allows pinpointing climate and drought influences on growth of coexisting conifers in continental Mediterranean climate. *Tree Physiology*. doi:10.1093/treephys/tpv125

Pan Y, Birdsey RA, Fang J *et al.* (2011) A large and persistent carbon sink in the world's forests. *Science (New York, N.Y.)*, **333**, 988–993.

Peguero-Pina JJ, Camarero JJ, Abadía A, Martín E, González-Cascón R, Morales F, Gil-Pelegrín E (2007) Physiological performance of silver-fir (*Abies alba* Mill.) populations under contrasting climates near the south-western distribution limit of the species. *Flora: Morphology, Distribution, Functional Ecology of Plants*, **202**, 226–236.

R Development Core Team (2014) *R: A Language and Environment for Statistical Computing*. R Foundation for Statistical Computing, Vienna, 409.

Sala A, Woodruff DR, Meinzer FC (2012) Carbon dynamics in trees: feast or famine? *Tree Physiology*, **32**, 764–775.

Sancho-Knapik D, Peguero-Pina J, Cremer E *et al.* (2014) Genetic and environmental characterization of *Abies alba* Mill. populations at its western rear edge. *Pirineos*, **169**, e007.

Sangüesa-Barreda G, Camarero JJ, Oliva J, Montes F, Gazol A (2015) Past logging, drought and pathogens interact and contribute to forest dieback. *Agricultural and Forest Meteorology*, **208**, 85–94.

Saurer M, Siegwolf RTW, Schweingruber FH (2004) Carbon isotope discrimination indicates improving water-use efficiency of trees in northern Eurasia over the last 100 years. *Global Change Biology*, **10**, 2109–2120.

Seibt U, Rajabi A, Griffiths H, Berry JA (2008) Carbon isotopes and water use efficiency: sense and sensitivity. *Oecologia*, **155**, 441–454.

Sevanto S, Mcdowell NG, Dickman LT, Pangle R, Pockman WT (2014) How do trees die? A test of the hydraulic failure and carbon starvation hypotheses. *Plant, Cell and Environment*, **37**, 153–161.

Sokal RR, Rohlf FJ (2012) *Biometry: the Principles and Practice of Statistics in Biological Research*, 4th edn. Freeman, New York, NY, USA.

Sperry JS, Love DM (2015) What plant hydraulics can tell us about responses to climate-change droughts. *New Phytologist*, **207**, 14–27.

Stephenson NL (1998) Actual evapotranspiration and deficit: biologically meaningful correlates of vegetation distribution across spatial scales. *Journal of Biogeography*, **25**, 855–870.

Trigo RM, Añel J, Barriopedro D *et al.* (2013) The record winter drought of 2011-12 in the Iberian Peninsula, in explaining extreme events of 2012 from a climate perspective. *Bulletin of the American Meteorological Society*, **94**, S41–S45.

Tyree MT, Zimmermann MH (2002) *Xylem Structure and the Ascent of Sap*, 2nd edn. Springer-Verlag, Berlin, Germany.

Vicente-Serrano SM, Camarero JJ, Zabalza J, Sangüesa-Barreda G, López-Moreno JI, Tague CL (2015) Evapotranspiration deficit controls net primary production and growth of silver fir: implications for circum-mediterranean forests under forecasted warmer and drier conditions. *Agricultural and Forest Meteorology*, **206**, 45–54.

von Wilpert K (1991) Intraannual variation of radial tracheid diameters as monitor of site specific water stress. *Dendrochronologia*, **9**, 95–113.

Wood SN (2006) *Generalized Additive Models: An Introduction With R*. Chapman and Hall/CRC. CRC, Boca Raton, FL.

Yazaki K, Maruyama Y, Mori S, Koike T, Funada R (2005) Effects of elevated carbon dioxide concentration on wood structure and formation in trees. In: *Plant Responses to Air Pollution and Global Change SE - 11* (eds Omasa K, Nouchi I, De Kok L), pp. 89–97. Springer Japan, Tokyo.

Supporting Information

Additional Supporting Information may be found in the online version of this article:

Figure S1. Changes in lumen area along the five tree-ring sectors.
Figure S2. Application of a Principal Componet Analysis to define earlywood and latewood from tree-ring sectors.
Figure S3. Observed changes in earlywood cell-wall thickness.
Figure S4. Nondeclining and declining Scots pine and silver fir correlations profiles.
Figure S5. Differences in earlywood lumen area of declining and nondeclining trees during years with contrasting water availability.
Table S1. Selection of best-fitted generalized additive models of earlywood lumen area for the two tree species.